IAHR AIRH
Taylor & Francis
Taylor & Francis Group

Journal of Hydraulic Research Vol. 48, No. 5 (2010), pp. 641–649
doi:10.1080/00221686.2010.512779

Research paper

Turbulent mixing of particles under tidal bores: an experimental analysis

HUBERT CHANSON (IAHR Member), Professor, *The University of Queensland, School of Civil Engineering, Brisbane QLD 4072, Australia*.
Email: h.chanson@uq.edu.au (author for correspondence)

KOK-KENG TAN, Graduate Student, *The University of Queensland, School of Civil Engineering, Brisbane QLD 4072, Australia.*
Email: kokkeng.tan@uqconnect.edu.au

ABSTRACT
A tidal bore develops in an estuary when the tidal range exceeds 4.5–6 m and the estuarine bathymetry amplifies the tidal wave. The bore is an abrupt rise in water depth associated with a discontinuity in velocity and pressure fields at the front. Herein the free-surface properties and the turbulent mixing of light-weight particles were investigated during the passage of tidal bores. The free-surface properties were recorded using a non-intrusive technique, while particle tracking was performed under undular and breaking bores. A basic result was the identification of a broad spectrum of particle trajectories, linked with the existence of large-scale vortical structures. These turbulent structures were responsible for the vertical water mixing as a tidal bore propagates upstream in an estuary. The large-scale eddies were also responsible for the rapid longitudinal dispersion of particulates, such as fish eggs, with some form of preferential motion, depending upon the particle's vertical elevation.

Keywords: Particle dispersion, physical modelling, tidal bore, turbulent mixing, unsteady flow

1 Introduction

A bore is an unsteady flow motion generated by the rapid water level rise at the river mouth during the early flood tide. With time, the leading edge of the tidal wave becomes steeper and steeper until it forms a wall of water, i.e. the tidal bore. After bore formation, there is an abrupt rise in water depth at the bore front, generating a discontinuity in water depth and velocity field. Figure 1 shows a tidal bore of Garonne River in south-western France. Once formed, the flow properties immediately before and after the tidal bore must satisfy the continuity and momentum principles (Rayleigh 1908, Henderson 1966, Liggett 1994). Their integral form of mass and momentum conservation gives a series of relations between the flow properties in front of and behind the bore front. For a rectangular horizontal channel and neglecting bed friction, it yields

$$\frac{d_{conj}}{d_o} = \frac{1}{2}\left(\sqrt{1 + 8\,\mathsf{F}^2} - 1\right) \tag{1}$$

where d_o is the initial water depth, d_{conj} the conjugate flow depth immediately after the bore passage, F the tidal bore Froude number defined as

$$\mathsf{F} = \frac{V_o + U}{\sqrt{g\,d_o}} \tag{2}$$

with V_o is the initial river flow velocity positive downstream and U the tidal bore celerity for an observer standing on the bank positive upstream (Fig. 2a). This Froude number is always larger than unity. For $\mathsf{F} < 1$, the tidal wave cannot become a tidal bore. For F slightly larger than unity, an undular bore is observed: the bore leading edge is followed by a train of secondary waves (Fig. 1). For larger F, a marked turbulent roller is seen, i.e. a breaking tidal bore.

Historically, major contributions on tidal bores include the works of Bazin (1865), Barré de Saint Venant (1871), Boussinesq (1877), Benjamin and Lighthill (1954) and Peregrine (1966). More recently, unsteady turbulence measurements were conducted using particle image velocimetry (PIV) and acoustic Doppler velocimetry (ADV) techniques (Hornung *et al.* 1995, Koch and Chanson 2009, Chanson 2010). The results indicate intense turbulent mixing during the tidal bore front passage. Herein, the free-surface properties and turbulent mixing of light

Revision received 30 July 2010/Open for discussion until 30 April 2011.

ISSN 0022-1686 print/ISSN 1814-2079 online
http://www.informaworld.com

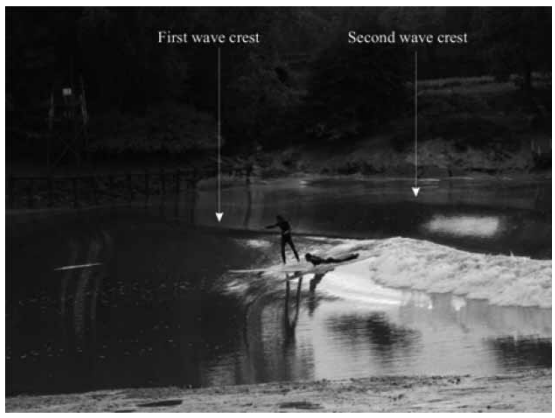

Figure 1 Photograph of undular tidal bore on Garonne River at Béguey, France, on 1 October 2008. Surfers ride ahead of first wave crest with bore propagating from right to left. Note the wave breaking in right foreground due to shallow water and first two wave crests in middle and right background

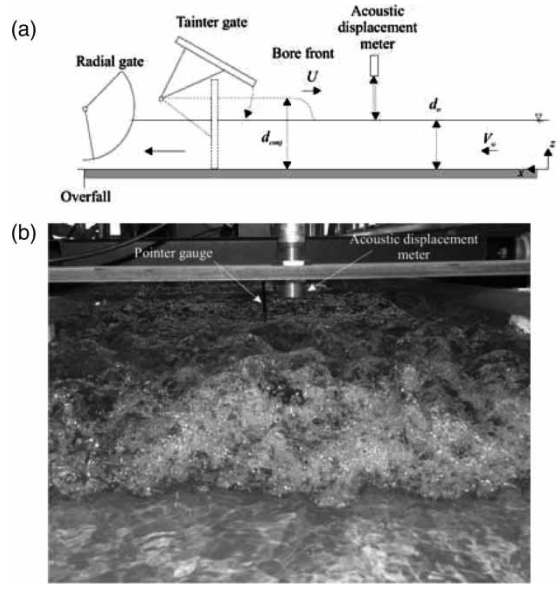

Figure 2 Experimental channel (a) definition sketch; (b) photograph of incoming front of breaking bore ($F = 1.5$, $Q = 0.058$ m^3/s, $d_o = 0.139$ m, shutter speed 1/80 s). Note the displacement meter sensor above bore front and pointer gauge in the background

particles were investigated during the passage of tidal bores. Particle tracking was conducted for both undular and breaking bores to provide a new Lagrangian description of the particle mixing processes. The results complement Eulerian velocity measurements performed in the same facility (Koch and Chanson 2009, Chanson 2010), and give a new understanding of the turbulent mixing of particles such as light-weight sediment or fish eggs.

2 Experimental facilities

2.1 *Presentation*

The experiments were performed in a 12 m long and 0.5 m wide rectangular open channel test section at the University of Queensland (Fig. 2). The flume was horizontal and made of smooth PVC bottom and glass walls. The water was supplied by a constant head tank feeding a large intake basin 2.1 m long, 1.1 m wide, 1.1 m deep, leading to the test section through a bottom and sidewall convergent. A radial gate was installed at the downstream channel end ($x = 11.9$ m, where x = longitudinal distance from channel upstream end), and the gate was used to control the initial water depth d_o. A fast-closing tainter gate was located at $x = 11.15$ m and was closed rapidly to generate a tidal bore propagating upstream (Fig. 2a).

The initially-steady discharge was measured with two orifice meters that designed upon the British Standards (1943). In steady flows, the water depths were measured using rail-mounted pointer gauges. The bore propagation was studied with a series of acoustic displacement meters Microsonic^{TM} Mic + 25/IU/TC located between $x = 10.8$ and 4 m and placed above the free surface (Fig. 2b). Further observations were recorded between $x = 5.65$ and 4.85 m using a digital video camera Panasonic NV-GS300 (30 fps) and digital still cameras.

2.2 *Particles and particle tracking experiments*

For one initial discharge, the turbulent mixing of particles was systematically investigated for both undular and breaking bores (Table 1). The particles were spherical-shaped beads of 3.72 $\pm$ 0.2 mm average diameter. Their relative density was deduced from particle fall velocity experiments conducted in a 2 m high, 0.10 m diameter water column filled with tap water, yielding a particle fall velocity of $w_s = 0.047 \pm 0.012$ m/s, corresponding to a relative particle density of $s = 1.037 \pm 0.012$.

The present particle shape, size and density were close to those of striped bass (*Morone saxatilis*) fish eggs. In the Bay of Fundy, the study of Rulifson and Tull (1999) reported fish egg diameters of about 4 mm with s between 1.0016 and 1.0066 depending upon their stages of development. Field observations indicated that the lightest eggs were unfertilized water-hardened eggs; fertilized eggs less than 10 h old had a relative density of 1.0029 and the heaviest eggs were in the final stages of development (Rulifson and Tull 1999). Herein the particles were injected on the channel centreline and advected downstream by the initially-steady flow. Their turbulent mixing in the bore front was recorded through the glass sidewall between $x = 5.65$ and 4.85 m using the video camera.

2.3 *Generation of tidal bores*

A range of experimental flow conditions was generated by changing independently three parameters: initially-steady discharge Q, initial flow depth d_o and tainter gate opening after closure (Table 1). The initially-steady discharges ranged from 0.013 to 0.058 m^3/s. For each test, the opening of the downstream radial gate controlled d_o. The radial gate position did not change during an experiment. The tidal bore was generated by

Table 1 Physical modelling and turbulence measurements in tidal bores

Reference (1)	Q (m^3/s) (2)	d_o (m) (3)	U (m/s) (4)	F (5)	Bed roughness (6)	Remarks (7)
Hornung *et al.* (1995)	0	–	–	1.5–6	Smooth	Rectangular channel
Koch and Chanson (2009)	0.040	0.079	0.14–0.68	1.3–2.0	Smooth PVC	$B = 0.5$ m
	0.058	0.137	0.56–0.9	1.17–1.5	Smooth PVC	$B = 0.5$ m
Chanson (2010)		0.142	0.50–0.9	1.1–1.5	Rough plastic screens	
Present study					Smooth PVC	$B = 0.5$ m
	0.013	0.0775	0.67	1.15		
		0.0505	0.55	1.51		Particle tracking experiments
	0.025	0.074	0.41–0.68	1.29–1.64		
		0.080	0.38–0.75	1.18–1.51		Free-surface measurements
		0.107	0.42–0.90	1.02–1.39		
		0.108	0.60–0.71	1.10–1.34		
		0.151	0.93–1.19	1.08–1.2		
	0.040	0.099	0.33–0.71	1.20–1.68		
		0.122	0.51–0.96	1.08–1.47		
		0.140	0.66–1.05	1.08–1.39		
		0.167	0.80–1.05	1.06–1.38		
		0.1835	0.90–1.18	1.01–1.23		
	0.058	0.1315	0.46–0.90	1.28–1.70		
		0.155	0.54–0.94	1.10–1.36		
		0.168	0.58–0.92	1.04–1.27		
		0.176	0.71–1.11	1.12–1.37		
		0.195	0.82–0.92	1.09–1.18		

Notes: B, channel width; d_o, initial water depth; F, tidal bore Froude number; Q, initially-steady discharge; U, tidal bore celerity; (–), data not available. All experiments were conducted with tap water

rapid closure of the downstream tainter gate. The gate was similar to that used by Koch and Chanson (2009) and Chanson (2010). Its closure time was recorded between 0.1 and 0.15 s, always less than 0.2 s. After rapid gate closure, the bore propagated upstream (Fig. 2), and each experiment was stopped when the tidal bore front reached the upstream intake structure ($x < 0$) to avoid wave reflection in the test section.

3. Basic flow patterns and free-surface characteristics

3.1 *Flow patterns*

Visual observations and free-surface measurements were conducted for a range of flow conditions with initially-steady subcritical open channel flow (Table 1). Figure 3 shows typical free-surface records for $F = 1.2$ and 1.56. Several flow patterns were observed depending upon the tidal bore Froude number. For $1 < F < 1.5$ to 1.6, the tidal bore was undular. The wave front was followed by a train of quasi-periodic waves called undulations (Figs. 1 and 3a). For larger F, a breaking bore was observed (Figs. 2b and 3b). The present observations were consistent with earlier findings of Favre (1935), Benet and Cunge (1971), Treske (1994) and Hornung *et al.* (1995).

The undular tidal bore had a smooth, quasi-two-dimensional (2D) free-surface profile for $F < 1.2$ to 1.25. For 1.2 to 1.25

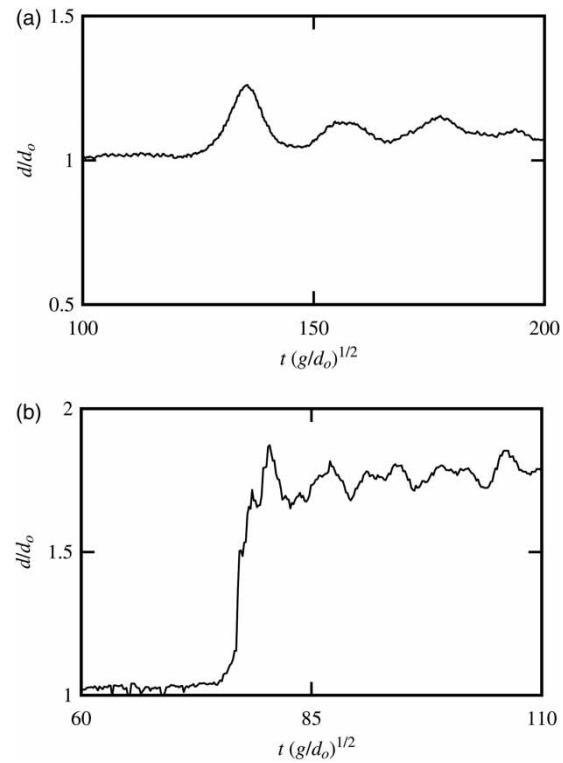

Figure 3 Dimensionless free-surface profiles of tidal bores at $x = 5$ m: (a) Undular tidal bore with $F = 1.20$, $Q = 0.025$ m^3/s, $d_o = 0.107$ m, $U = 0.73$ m/s, (b) Breaking tidal bore with $F = 1.56$, $Q = 0.058$ m^3/s, $d_o = 0.1315$ m, $U = 0.99$ m/s

$< \mathsf{F}$, slight cross-waves (shock waves) were observed, starting next to the sidewalls upstream of the first wave crest and intersecting next to the first crest on the channel axis. For $1.35 < \mathsf{F} < 1.5$ to 1.6, some slight wave breaking was observed at the first wave crest, and the secondary waves were flatter. These findings are comparable to those of Koch and Chanson (2009) and Chanson (2010). For $\mathsf{F} > 1.5$ to 1.6, the bore had a marked roller, and appeared to be quasi-2D. Behind the roller, the free-surface was about horizontal although large free-surface fluctuations were observed (Fig. 3b). Air entrainment and intense turbulent mixing was observed in the bore roller. Note that the flow patterns were basically independent of Q and d_o, while an earlier study showed that these were also independent of bed roughness (Chanson 2010).

3.2 *Free-surface properties*

In a tidal bore, the ratio of water depths d_{conj}/d_o has to satisfy Eq. (1). The experimental data are regrouped in Fig. 4, where the ratio of the conjugate depths is plotted versus F. The present data were compared with those of the earlier studies including a field experiment. The data trend was close to that predicted by the momentum principle, although Eq. (1) was developed by assuming hydrostatic pressure distribution. This approximation is inaccurate for undular bores since the pressure distribution deviates from hydrostatic because of streamline curvature (Rouse 1946, Montes and Chanson 1998, Cunge 2003).

A key feature of undular tidal bores is the quasi-periodic appearance of secondary waves (Figs. 1 and 3a). Herein the characteristics of the undulations were systematically recorded for $Q = 0.025$, 0040, 0.058 m^3/s, and for a range of initial flow depths (Table 1). Typical results are shown in Figs. 5

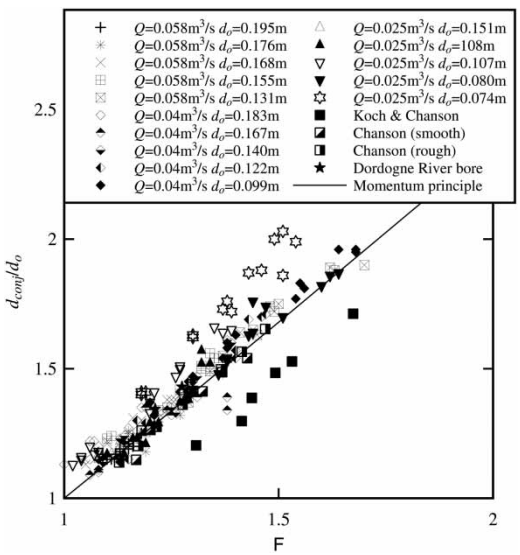

Figure 4 Ratio of conjugate depths in tidal bores, comparison between present data, Eq. (1), earlier laboratory studies (Koch and Chanson 2009, Chanson 2010) and prototype study on Dordogne River (Navarre 1995)

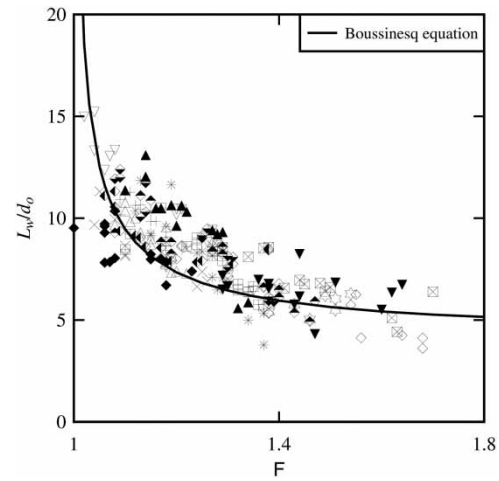

Figure 5 Dimensionless wave length L_w/d_o of first wave length for undular tidal bores, comparison between present data and Boussinesq equation (Andersen 1978). Legend as in Fig. 4

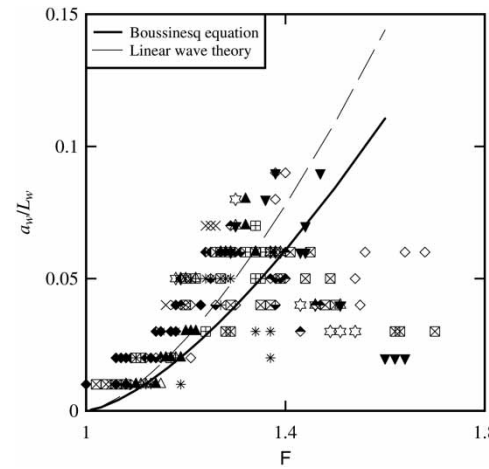

Figure 6 Dimensionless wave steepness a_w/L_w of first wave length of undular tidal bores, Comparison between present data, Boussinesq equation (Andersen 1978) and the linear wave theory (Lemoine 1948). Legend as in Fig. 4

and 6 in terms of the dimensionless wave length L_w/d_o and steepness a_w/L_w, where a_w and L_w are the wave amplitude and length, respectively. The present experimental data are compared with the linear wave theory and the Boussinesq equation solutions (Lemoine 1948, Andersen 1978) in Figs. 5 and 6. There is reasonable agreement between the data and the theoretical developments, although the wave steepness data are closer to the linear wave theory. While the wave length decayed exponentially with increasing F, the wave steepness data exhibited a local maximum at about $\mathsf{F} = 1.3$–1.4. It is believed that the apparition of slight breaking at the first wave crest for $\mathsf{F} > 1.35$ is responsible for reduced energy dissipation in the secondary wave motion at larger F and hence the smaller wave steepness for $\mathsf{F} > 1.3$–1.4. An important finding was independence of the results from the initially-steady Froude number (Figs 4–6). The free-surface properties are basically independent of the initial water depth and velocity within the test range (Table 1).

4 Particle trajectories

4.1 *Trajectory patterns*

For one discharge, the dispersion of light-weight particles was investigated in both undular and breaking tidal bores (Table 1). The particle trajectories were observed at $x \cong 5$ m. Typical particle trajectories are shown in Figs. 7 and 8 for the undular and breaking tidal bores, respectively, in dimensionless form. For each trajectory, the horizontal axis is the longitudinal distance x' positive downstream with $x' = 0$ as the particle passed underneath the leading edge of the bore front and the vertical axis = vertical particle elevation z. The time interval between each data point is $1/30$ s, with the tidal bore propagating from right to left.

In the undular bore, particle trajectories highlight two distinct trends. For the particles flowing initially in the upper flow region $z_o/d_o > 0.5$, a relatively significant proportion follows a helicoidal pattern (Fig. 7, particles 6a, 6c, 6d, 8b). These followed an orbital path beneath the wave crest, reaching their maximum vertical elevation just below the wave crests. Between wave crests, these particles were advected in the downstream direction as they passed underneath each wave trough. The particle orbital trajectories are comparable to particle trajectories observed below regular waves (Sawaragi 1995), although the entire particle motion appeared to be a combination of orbital paths and downstream advection. Further regular waves cause only mild mixing, which is different from the intense mixing induced by the tidal bore. As the particles flowed initially close to the bed ($z_o/d_o < 0.5$), they were subjected to recirculation consisting of an initially rapid deceleration followed by an upstream advection close to the bed behind the bore front. For example, in Fig. 7, particles 2, 4c and 5b were recirculated upstream with an advective velocity $V_x/V_o = -0.5$ in average. The two distinctive patterns are seen in Fig. 7.

In the breaking bore, the particle trajectory motion was more complex. Most particles travelling initially next to the channel bed ($z_o/d_o < 0.2$) were subjected by a sudden deceleration followed by an upstream motion, e.g. particle trajectory b8 with white circular symbols in Fig. 8. The other particle trajectories exhibited a pseudo-chaotic motion induced by the large-scale turbulent eddies generated in the mixing layer of the bore roller. Some examples of such particle trajectories are presented in Fig. 8 (e.g. particles b2a, b6a, b9b, b10c). Note that the experiments were conducted for a relatively small Froude number for which the air entrainment in the breaking bore roller was negligible and did not affect adversely the particle tracking accuracy.

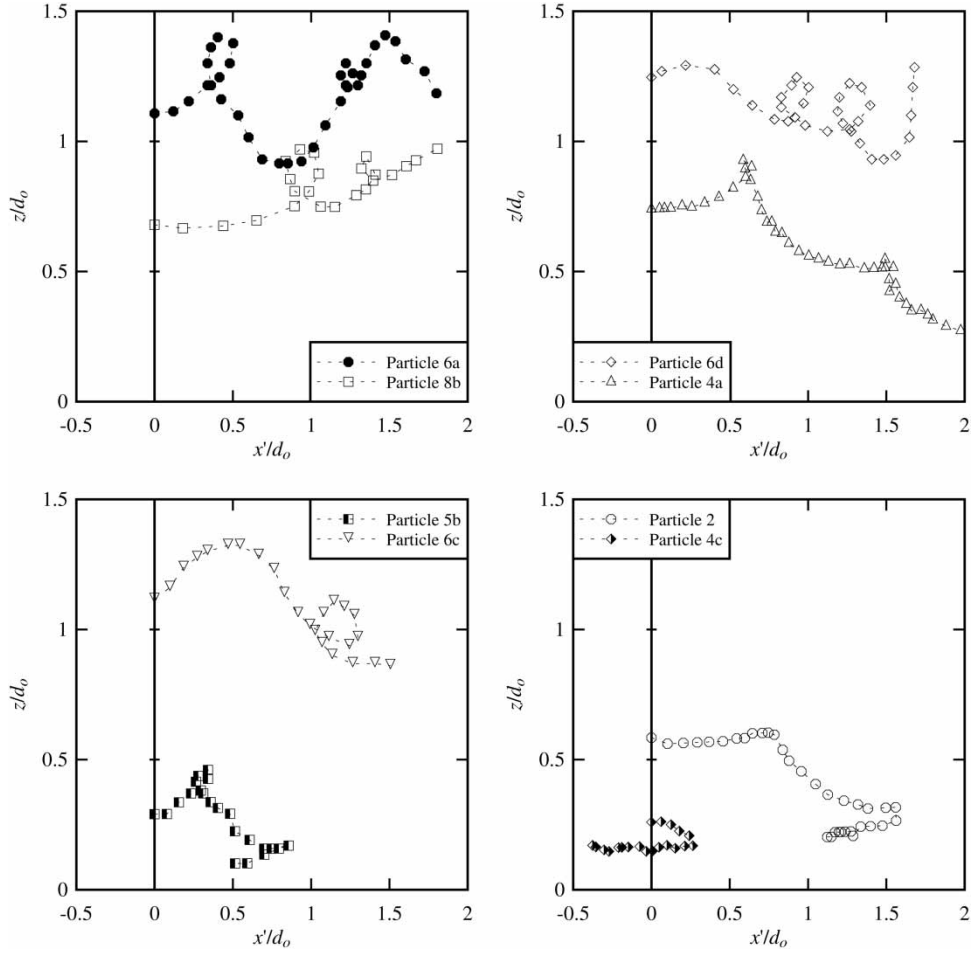

Figure 7 Dimensionless particle trajectories in undular tidal bore for F = 1.15, $Q = 0.013$ m^3/s, $d_o = 0.0775$ m. Bore propagation from right to left

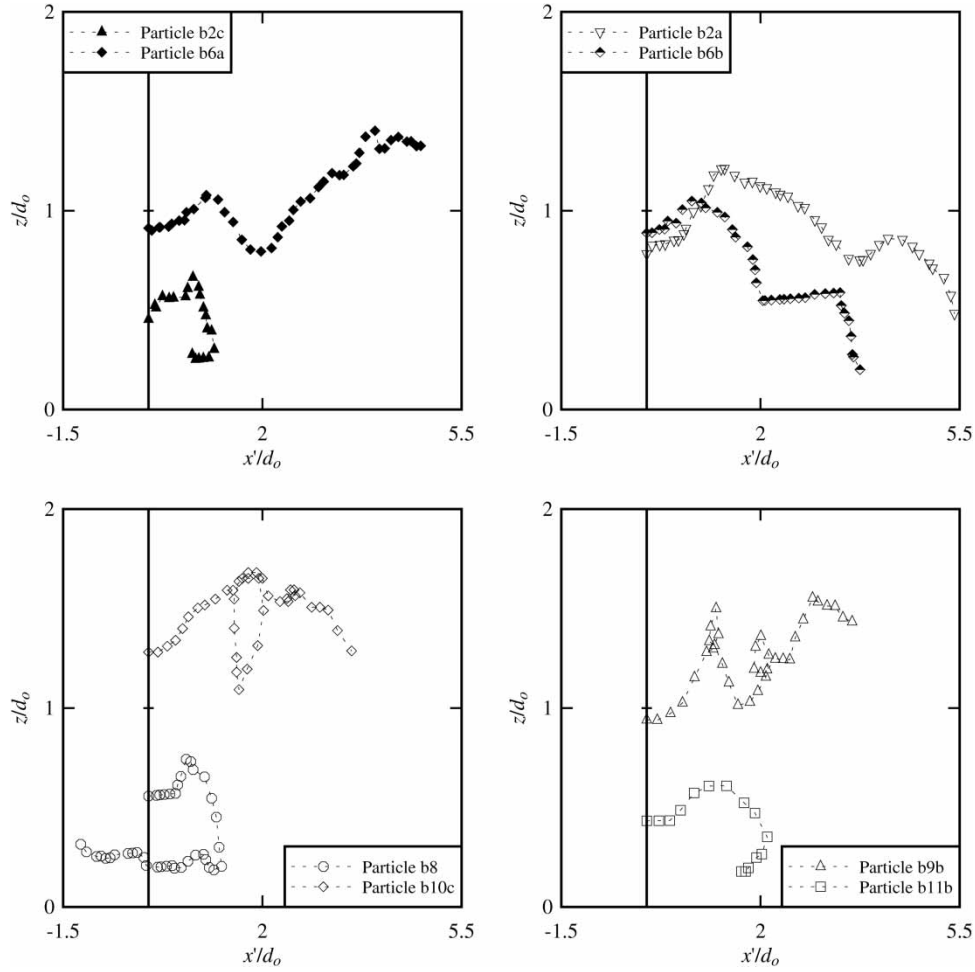

Figure 8 Dimensionless particle trajectories in breaking tidal bore for $\mathsf{F} = 1.51$, $Q = 0.013$ m^3/s, $d_o = 0.0505$ m. Bore propagation from right to left

4.2 *Particle mixing*

Observations showed qualitatively a rapid mixing of particles during tidal bore passage. Assuming a homogenous, steady turbulence behind the bore front, the turbulent diffusion coefficient of the particles may be estimated from their mean square displacement to

$$D_x = \frac{\sigma_x^2}{2\,t'} \tag{3}$$

$$D_z = \frac{\sigma_z^2}{2\,t'} \tag{4}$$

where D_x and D_z is the turbulent mixing coefficients of the particles in the x- and z-directions, respectively, σ_x and σ_z the mean square displacement of the particles in the x- and z-directions, respectively, and t' the time scale with $t' = 0$ when the particle passed beneath the leading edge of the bore front. Equations (3) and (4) may be derived using Langevin's model of turbulent dispersion or the random walk model assuming that t' is much larger than the Lagrangian time scale (Pope 2000, Chanson 2004). Simply D_x and D_z characterize the turbulent diffusion of the light-weight particles immediately behind the tidal bore front within the simplistic approximations of homogeneous turbulence and vertically-mixed water column.

The dimensionless results are summarized in Table 2. Despite the simplistic assumptions underlying Eqs. (3) and (4), the data suggest that the longitudinal mixing coefficient is nearly one order of magnitude larger than the vertical mixing coefficient (Table 2). Further, the undular bore induces larger vertical mixing than the breaking bore, because it is linked to the streamline pattern induced by the free-surface undulations. For comparison, the average vertical mixing coefficient in a fully-developed open channel is

$$\frac{\varepsilon_z}{V_o d_o} = 0.067\sqrt{\frac{f}{8}} \tag{5}$$

where f is the Darcy–Weisbach friction factor (Rutherford 1994, Chanson 2004). For a smooth flume, it yields $\varepsilon_z/(V_o d_o) \approx 0.003$ to 0.004. The present data imply that the vertical diffusion coefficients behind tidal bores were one order of magnitude larger than the vertical diffusion coefficient in a fully-developed, steady open channel flow. Overall the experimental data indicate a strong longitudinal and vertical mixing during the

Table 2 Turbulent mixing coefficients of light-weight particles immediately behind tidal bores

Tidal bore (1)	V_o (m/s) (2)	d_o (m) (3)	$D_x/(V_o d_o)$ (4)	$D_z/(V_o d_o)$ (5)	Remark (6)
Undular	0.335	0.0775	0.10	0.018	For $t\sqrt{g/d_o} < 14$
Breaking	0.515	0.0505	0.12	0.011	

tidal bore passage with moderate differences between undular and breaking tidal bores (Table 2).

5 Discussion

The present findings demonstrated a broad spectrum of particle trajectories and patterns during the passage of a tidal bore (Figs. 7 and 8). Both qualitative and quantitative observations imply the existence of large-scale vortices in which the particles are trapped and advected within. Earlier physical and numerical studies document the production of large coherent structures in tidal bores (Koch and Chanson 2009, Lubin *et al.* 2010). The existence of energetic turbulent events beneath and shortly beyond the tidal bore front imply the generation of vorticity during bore propagation. The presence of these persisting coherent structures indicates that a great amount of sediment material could be placed into suspension and transported by the main flow in a natural system. The present observations with light-weight particles suggest that the tidal bore process contributes efficiently to the longitudinal dispersion of eggs, reducing the efficiency of predators in tidal-bore affected estuaries, as proposed by Morris *et al.* (2003). Beneath an undular tidal bore, the particle motion data yield relatively large fluctuations of horizontal and vertical particle velocity components below undulations. The long-lasting impact of the free-surface undulations is a key feature of undular tidal bores in natural systems (Koch and Chanson 2008). The comparative observations with a same initial discharge suggest that undular bores induce a larger particle mixing as compared with breaking bores, especially in the upper flow region ($z_o/d_o > 0.5$) (Table 2, column 5).

The present results may provide a better understanding of the impact of tidal bore on fish eggs in a tidal bore-affected estuary. In the natural system, fish eggs are typically advected downstream by the ebb tide. The arrival of a tidal bore does induce a marked longitudinal spread of the eggs. Those located in the upper flow region continue to flow downstream, while the others reverse their course being re-directed upstream behind the bore. The tidal bore induces a rapid longitudinal spread of the eggs under preferential motion, depending upon their vertical position in the water column. The lowest, typically heaviest fish eggs are advected upstream immediately after the tidal bore passage. The higher, typically neutrally buoyant eggs located next to the surface continue their journey downstream for sometimes, although the strong flood flow may bring them back into the upper estuary at a later stage of the tide.

6 Conclusions

This study investigates turbulent mixing of light-weight particles in a tidal bore. Herein the small particles had physical properties close to striped bass fish eggs, and their turbulent dispersion associated with the passage of undular and breaking bores was documented experimentally.

The free-surface properties were investigated for a range of initial flow conditions. The findings suggest that these have a small effect on the tidal bore characteristics. The undular wave steepness data highlight a local maximum for $\mathsf{F} = 1.3–1.4$ that was associated with the apparition of breaking at the first wave crest, and the disappearance of the secondary waves for $\mathsf{F} > 1.5–1.6$. The results highlight that the initial flow conditions have a small effect on the dimensionless free-surface properties.

The particle trajectory data complement earlier experimental and numerical results. They indicate, in particular, rapid particle deceleration and reversal beneath the bore front. Large fluctuations of horizontal and vertical particle velocities were observed during undular bore passage and beneath the ensuing undulations. Seminal features were highlighted, including large-scale motion highlighting the existence of large coherent vortical structures. These are responsible for bed erosion and vertical mixing of the water column as a tidal bore propagates upstream in the estuarine zone of a natural system. The large-scale vortices are also responsible for the longitudinal dispersion of fish eggs reducing the impact of predators. The present results indicate that the tidal bore induces a rapid longitudinal spread of the eggs with a preferential motion depending upon their initial vertical elevation. Finally, it must be noted that the present experiments were performed with a unique particle size and density. Future tests should encompass a range of particle sizes and density.

Acknowledgements

The authors acknowledge the technical assistance of Graham Illidge and Clive Booth, University of Queensland.

Notation

a_w = amplitude of first wave length (m)
B = channel width (m)
d = flow depth measured normal to invert (m)
D_x = turbulent mixing coefficient in x-direction (m^2/s)

D_z = turbulent mixing coefficient in z-direction (m^2/s)
F = tidal bore Froude number (–)
f = Darcy–Weisbach friction factor (–)
g = gravity constant (m/s^2)
L_w = first wave length (m)
Q = discharge (m^3/s)
s = relative particle density (–)
t = time (s)
t' = time, with $t' = 0$ as particle passed beneath bore front (s)
U = bore front celerity (m/s)
V = velocity (m/s)
V_o = initial flow velocity (m/s)
w_s = particle fall velocity (m/s)
x = longitudinal distance measured from channel upstream end (m)
x' = longitudinal distance, with $x' = 0$ when particle passed beneath bore front (m)
z = particle elevation above invert (m)
z_o = initial particle elevation above invert at $t' = 0$ (m)
ε_z = vertical mixing coefficient in fully-developed open channel flow (m^2/s)
σ_x = mean square displacement of particles in x-direction (m)
σ_z = mean square displacement of particles in z-direction (m)

Subscript

conj = conjugate flow condition
o = initial flow conditions prior to bore passage
x = longitudinal component
z = vertical component

References

Andersen, V.M. (1978). Undular hydraulic jump. *J. Hydraulics Division* ASCE 104(HY8), 1185–1188. Discussion: 105(HY9), 1208–1211.

Barré de Saint-Venant, A.J.C. (1871). Théorie du mouvement non permanent des eaux, avec application aux crues des rivières et à l'introduction des marées dans leur lit. (Theory of unsteady flow motion, including applications to floods and tidal effect). *Comptes Rendus des séances de l'Académie des Sciences*, Paris, France 73(4), 147–154 [in French].

Bazin, H. (1865). Recherches expérimentales sur la propagation des ondes (Experimental research on wave propagation). *Mémoires présentés par divers savants à l'Académie des Sciences* Paris, France 19, 495–644 [in French].

Benet, F., Cunge, J.A. (1971). Analysis of experiments on secondary undulations caused by surge waves in trapezoidal channels. *J. Hydraulic Res.* 9(1), 11–33.

Benjamin, T.B., Lighthill, M.J. (1954). On cnoidal waves and bores. *Proc. Royal Soc.* London, Series A, 224(1159), 448–460.

Boussinesq, J.V. (1877), Essai sur la théorie des eaux courantes (Essay on the theory of water flow). *Mémoires présentés par divers savants à l'Académie des Sciences* Paris, France 23, 1–680; 24, 1–60 [in French].

British Standard (1943). Flow measurement. *British Standard Code BS* 1042:1943. British Standard Institution, London.

Chanson, H. (2004). *Environmental hydraulics of open channel flows*. Elsevier-Butterworth-Heinemann, Oxford UK.

Chanson, H. (2010). Unsteady turbulence in tidal bores: Effects of bed roughness. *J. Waterway, Port, Coastal, and Ocean Engineering* 136(5), 247–256.

Cunge, J.A. (2003). Undular bores and secondary waves: Experiments and hybrid Finite-Volume modelling. *J. Hydraulic Res.* 41(5), 557–558.

Favre, H. (1935). *Etude théorique et expérimentale des ondes de translation dans les canaux découverts* (Theoretical and experimental study of travelling surges in open channels). Dunod, Paris [in French].

Henderson, F.M. (1966). *Open channel flow.* MacMillan, New York.

Hornung, H.G., Willert, C., Turner, S. (1995). The flow field downstream of a hydraulic jump. *J. Fluid Mech.* 287, 299–316.

Koch, C., Chanson, H. (2008). Turbulent mixing beneath an undular bore front. *J. Coastal Res.* 24(4), 999–1007.

Koch, C., Chanson, H. (2009). Turbulence measurements in positive surges and bores. *J. Hydraulic Res.* 47(1), 29–40.

Lemoine, R. (1948). Sur les ondes positives de translation dans les canaux et sur le ressaut ondulé de faible mmplitude (On the positive surges in channels and on the undular jumps of low wave height). *J. La Houille Blanche* 4(3/4), 183–185 [in French].

Liggett, J.A. (1994). *Fluid mechanics*. McGraw-Hill, New York.

Lubin, P., Glockner, S., Chanson, H. (2010). Numerical simulation of a weak breaking tidal bore. *Mechanics Res. Comm.* 37(1), 119–121.

Montes, J.S., Chanson, H. (1998). Characteristics of undular hydraulic jumps: Results and calculations. *J. Hydraulic Eng.* 124(2), 192–205.

Morris, J.A., Rulifson, R.A., Toburen, L.H. (2003). Life history strategies of striped bass, *Morone saxatilis*, populations inferred from otolith microchemistry. *Fisheries Res.* 62(1), 53–63.

Navarre, P. (1995). Aspects physiques du caractère ondulatoire du macaret en Dordogne (Physical features of the undulations of the Dordogne River tidal bore). *D.E.A. thesis*, Univ. of Bordeaux, France [in French].

Peregrine, D.H. (1966). Calculations of the development of an undular bore. *J. Fluid Mech.* 25, 321–330.

Pope, S.B. (2000). *Turbulent flows*. Cambridge University Press, Cambridge UK.

Rayleigh Lord (1908), Note on tidal bores. *Proc. Royal Soc.* London, Series A 81(541), 448–449.

Rouse, H. (1946). *Elementary mechanics of fluids*. Wiley, New York.

Rulifson, R.A., Tull, K.A. (1999). Striped bass spawning in a tidal bore river: The Shubenacadie Estuary, Atlantic Canada. *Trans. American Fisheries Soc.* 128(4), 613–624.

Rutherford, J.C. (1994). *River mixing*. Wiley, Chichester UK.

Sawaragi, T. (1995), *Coastal engineering*: Waves, beaches, wave-structure interactions, Developments in Geotechnical Engineering, Series, No. 78. Elsevier, Amsterdam NL.

Treske, A. (1994). Undular bores (Favre-waves) in open channels: Experimental studies. *J. Hydraulic Res.* 32(3), 355–370. Discussion: 33(3), 274–278.